ISSN 1063-7834, Physics of the Solid State, 2016, Vol. 58, No. 7, pp. 1453–1457. © Pleiades Publishing, Ltd., 2016.
Original Russian Text © A.D. Pogrebnjak, A.A. Dem'yanenko, V.M. Beresnev, O.V. Sobol', O.M. Ivasishin, K. Oyoshi, Y. Takeda, H. Amekura, A.I. Kupchishin, 2016, published in Fizika Tverdogo Tela, 2016, Vol. 58, No. 7, pp. 1403–1407.

SURFACE PHYSICS AND THIN FILMS

Recrystallization and Formation of Spheroidal Gold Particles in Amorphous-Like AlN–TiB_2–$TiSi_2$ Coatings after Annealing and Subsequent Implantation

A. D. Pogrebnjak[a, *], A. A. Dem'yanenko[a], V. M. Beresnev[b], O. V. Sobol'[c], O. M. Ivasishin[d], K. Oyoshi[e], Y. Takeda[e], H. Amekura[e], and A. I. Kupchishin[f]

[a] *Sumy State University, ul. Rimskogo-Korsakova 2, Sumy, 40007 Ukraine*

[b] *Karazin Kharkiv National University, pl. Svobody 4, Kharkiv, 61022 Ukraine*

[c] *National Technical University "Kharkiv Polytechnic Institute," ul. Frunze 21, Kharkiv, 61002 Ukraine*

[d] *Kurdyumov Institute for Metal Physics, National Academy of Sciences of Ukraine, bulv. Akademika Vernadskogo 36, Kyiv, 03680 Ukraine*

[e] *National Institute for Materials Science (NIMS), 3-13 Sakura, Tsukuba, Ibaraki Prefecture, 305-0047 Japan*

[f] *Kazakh National Pedagogical University named after Abai, pr. Dostyk 13, Almaty, 050010 Republic of Kazakhstan*

** e-mail: alexp@i.ua*

Received April 14, 2015; in final form, December 30, 2015

Abstract—The recrystallization of the structure of an X-ray amorphous AlN–TiB_2–$TiSi_2$ coating containing short-range order regions with characteristic sizes of 0.8–1.0 nm has been performed using a negative gold ion (Au^-) beam and high-temperature annealing. Direct measurements using methods of high-resolution transmission electron microscopy (HRTEM) and energy-dispersive X-ray spectral (EDXS) microanalysis have demonstrated that thermal annealing at a temperature of 1300°C in air results in the formation of nanoscale (10–15 nm) phases AlN, AlB_2, Al_3O_3, and TiO_2, whereas the ion implantation of negative ions Au^- leads to a fragmentation (decrease in the size) of nanograins to 2–5 nm with the formation of spheroidal gold nanocrystallites a few nanometers in size, as well as to the formation of an amorphous oxide film in the depth (near-surface layer) of the coating due to ballistic ion mixing and collision cascades.

DOI: 10.1134/S1063783416070283

1. INTRODUCTION

Nanocomposites represent a new generation of materials both due to small grain sizes ($\leqslant$10 nm) and due to a significant role of boundary regions surrounding individual grains [1–3]. Nanocomposite coatings exhibit improved properties and behave in a completely different manner with respect to conventional materials with greater grain sizes ($\geqslant$100 nm) [3–7].

A desired combination of the high rate of coating deposition and the high accuracy of reproducible composition can be achieved using the magnetron sputtering method. The ion implantation of intense beams of negative ions with appropriate types of accelerators makes it possible to purposefully change properties of materials in a local region [8], for example, by doping of dielectrics (SiO_2) with the purpose of generating radiation in the ultraviolet range (using luminescence), where emission centers are nanoparticles formed from negative gold ions and copper ions due to the implantation [9].

An obvious advantage of negative ions is that a dielectric material implanted with these ions does not acquire a charge. Moreover, nanocomposites (or nanomaterials), along with a high hardness (and, simultaneously, with a high plasticity), should exhibit a high resistance to thermal oxidation. The formation of an amorphous-like structure in multicomponent (gradient) coatings is also an important factor that is responsible for their high functional properties and determines a high diffusion resistance to external influences due to the absence of easy diffusion paths in an amorphous matrix. Naturally, in this case, amorphous-like structures are thermodynamically metastable, and, therefore, another important factor for their transformation is high-temperature annealing. At the same time, implantation of heavy ions with high doses of up to 10^{17} ions/cm^{-2} into an amorphous–

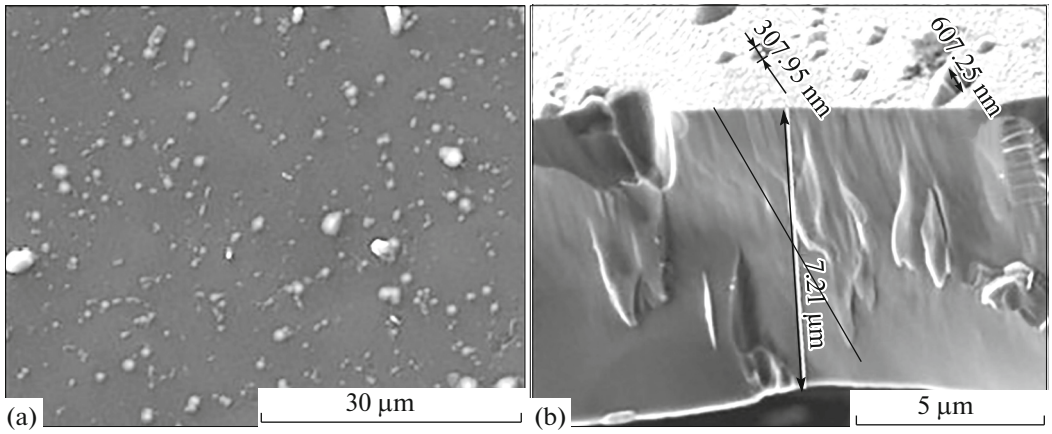

Fig. 1. (a) Topography and (b) fractography of the fracture of the AlN–TiB_2–$TiSi_2$ coating.

nanocrystalline structure of coatings has not been investigated in sufficient detail.

Therefore, the purpose of this work was to investigate the processes occurring in the microstructure of amorphous-like and nanocomposite coatings based on the AlN–TiB_2–$TiSi_2$ composition due to high-temperature annealing up to 1300°C, as well as to analyze the influence of the microstructure on the mechanical properties of these coatings and the possibility of the formation of spheroidal gold nanoclusters as a result of the implantation of negative gold ions (Au^-).

2. SAMPLE PREPARATION AND EXPERIMENTAL TECHNIQUE

The coatings were deposited onto polished samples of molybdenum and silicon by pulsed magnetron sputtering of a target with the complex composition AlN–TiB_2–$TiSi_2$ (where the content of the AlN phase was 30 vol %), owing to which high-quality nanocomposites have been fabricated in recent years [5–9]. The thickness of the coatings and the state of the boundaries between the substrate and the coating were determined from the fractographs of the fractures measured using scanning electron microscopy on a Quanta 600 FEG scanning ion-electron microscope. The surface morphology of the samples was also examined using scanning electron microscopy with the energy-dispersive X-ray spectral (EDXS) microanalysis on a JEOL-7000F scanning electron microscope. The structure and substructure of the samples with coatings were investigated using the small-angle X-ray scattering method in CrK_α radiation on a Rigaku RINT-2500V diffractometer. The X-ray diffraction spectra were measured at angles of 2°, 3°, 10°, and 30°. In addition, the substructure was investigated using high-resolution transmission electron microscopy (HRTEM) on a JEOL JEM-2100F field-emission transmission electron microscope in the bright and dark fields (the electron energy was 200 keV).

Negative ions Au^- were generated by a special Cs-assisted plasma-sputter-type ion source (Nissan High Voltage Co. Ltd). An intense ion beam of negative ions was formed using two electrodes and accelerated to 60 keV (the Au^- ion beam current was 4 mA).

3. RESULTS AND DISCUSSION

The topography and fractograph of the fracture of the AlN–TiB_2–$TiSi_2$ coating with a thickness of approximately 7 μm are shown in Figs. 1a and 1b, respectively. The principles of the design of magnetron sputtering devices make it possible to solve sufficiently easily the problem of the deposition of uniform coatings containing characteristic droplet inclusions with sizes of up to 300–600 nm.

The results of the elemental composition of the AlN–TiB_2–$TiSi_2$ coatings in the initial state and in the

Elemental composition of the AlN–TiB_2–$TiSi_2$ coatings

Composition	Elements involved in the composition of the AlN–TiB_2–$TiSi_2$ coatings, at %						
	B	C	O	N	Al	Si	Ti
Initial	34.49	17.27	11.92	9.26	17.25	2.89	6.92
After annealing at 900°C	38.07	12.70	13.14	8.32	18.30	2.70	6.72
After annealing at 1300°C	23.57	30.36	26.84	6.97	11.45	0.32	0.49

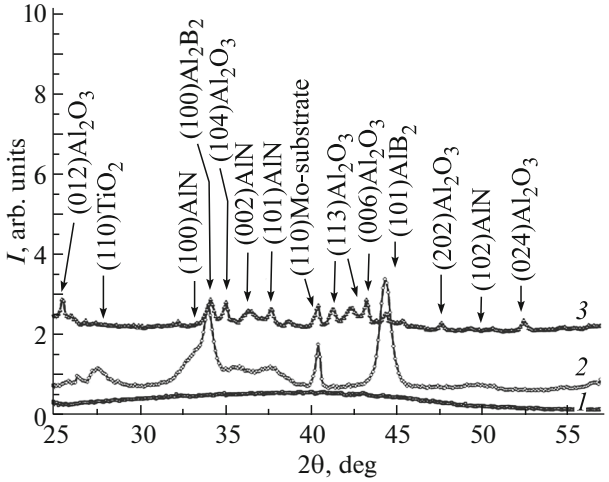

Fig. 2. Fragments of the X-ray diffraction patterns obtained for the AlN–TiB_2–$TiSi_2$ coatings: (*1*) the initial state, (*2*) after thermal annealing at a temperature of 900°C in air, and (*3*) after annealing at 1300°C.

state after annealing at temperatures of 900°C and 1300°C are presented in the table. It can be seen from this table that an increase in the annealing temperature leads to a decrease in the concentrations of elements in the following ranges: from 34 to 23.37 at % for boron, from 9.26 to 6.97 at % for nitrogen, from 17.25 to 14.45 at % for aluminum, from 2.89 to 0.32 at % for silicon, and from 6.92 to 0.49 at % for titanium. At the same time, the concentrations of carbon and oxygen increase in the ranges from 17.27 to 30.36 at % and from 11.52 to 26.84 at %, respectively.

The results of the X-ray diffraction analysis (Fig. 2) demonstrate that the coatings formed during the deposition have an X-ray amorphous structure, which is also confirmed by the results of the TEM and HRTEM measurements. The X-ray diffraction patterns in the angle ranges $2\theta \approx 30°–50°$ and 65°–75° exhibit a halo with a maximum (in the absence of clear diffraction maxima). The size of short-range order

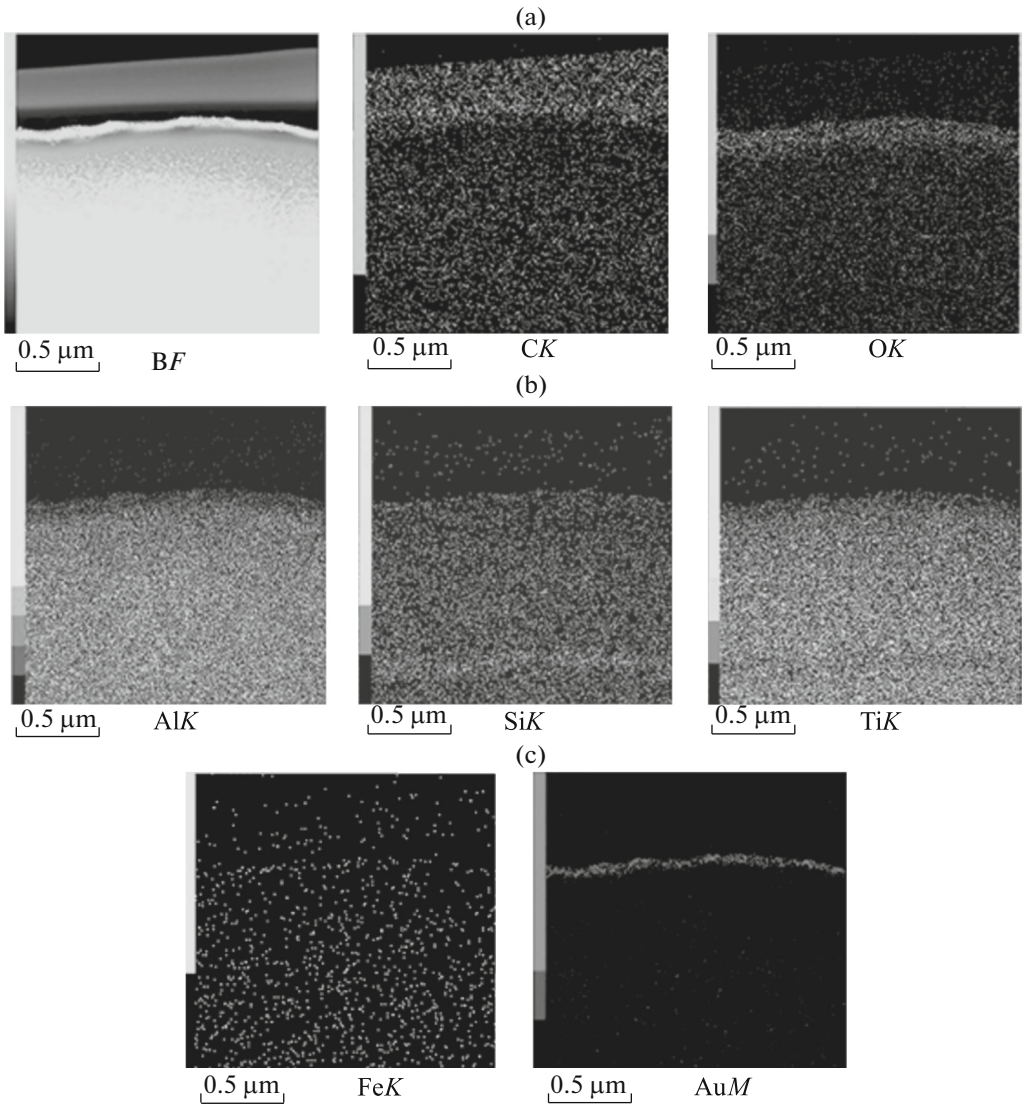

Fig. 3. Cross-sectional elemental distribution maps: (a) B, C, and O; (b) Si, Al, and Ti; and (c) Fe and Au.

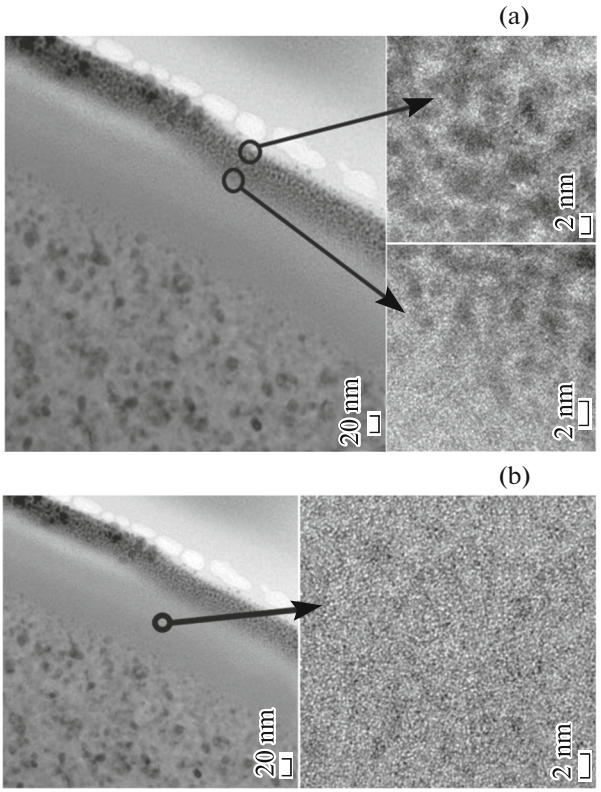

Fig. 4. Results of the TEM and HRTEM analyses with an atom-by-atom resolution of the selected regions with the selected area diffraction: (a) image of gold clusters near the surface layer and (b) image of the oxide layer.

regions in the coatings can be estimated according to the relationship

$$R_m \approx 10/\Delta s. \quad (1)$$

Here, R_m is the correlation radius and Δs is the width of the first wide-angle "halo-shaped" curve in the "intensity–scattering vector s" coordinates (where $s = |\underline{s}| = 4\pi\sin\theta/\lambda$ is the magnitude of the scattering vector). This estimation shows that the short-range order regions have the size $R_m \sim 10$ Å ~ 1 nm.

It should be noted that expression (1) follows from the fact that the correlation radius (the size of the short-range order regions) is inversely proportional to the magnitude of the scattering vector s:

$$R_m = 2\pi \exp 3z \exp 2/6.25\Delta s, \quad (2)$$

where z is the index of the maximum. For the first maximum ($z = 1$), we have $R_m \approx 10/\Delta s$.

The annealing of the coating at a higher temperature of 1300°C leads to a fundamental change in the X-ray diffraction pattern. It can be seen from Fig. 2 that, in the coating, there occurs the formation of nanoscale phases, namely, a relatively large amount of aluminum oxide Al_2O_3, a significantly smaller amount of AlB_2, and small amounts of TiO_2, AlN, and "possibly" SiO_2. The formation of Al_2O_3 and AlB_2 crystallites, in this case, is caused by the highest heat of formation, which is characteristic of these phases. It should be noted that, both in the case of annealing at 900°C and in the case of annealing at 1300°C, the surface of the coating is depleted in the boride phase. Moreover, after the irradiation with Au^- ions (due to the etching–sputtering of the surface and a lower binding energy), the percentage of borides is also reduced, as can be seen from a relative decrease of the heights of the peaks attributed to aluminum diboride. There is also a decrease in the roughness of the surface of the coating, which is manifested in a relatively low spread of the background of the X-ray diffraction pattern recorded in the glancing-angle geometry. However, it can also be seen that a thin amorphous oxide film is formed near the surface (Figs. 3a, 4b).

The results of the elemental analysis of the composition in the form of cross-sectional elemental distribution maps of the sample in elemental contrast and in the bright field are presented in Figs. 3a–3c. It can be seen from these maps that C, Al, Ti, Si, and B are uniformly distributed, except for the surface, and a greater amount of oxygen is located near the surface (at a depth of 40–100 nm). There is also a clearly visible Au^- trace, which lies at the depth of the coating with a concentration of approximately 0.4 at %.

According to the visualizing data of the high-resolution transmission electron microscopy (Figs. 4a, 4b), after the high-temperature annealing and subsequent ion implantation, three characteristic zones are formed in the coating. Near the surface, there is a 40-nm-thick implantation zone with doping by implanted gold. Owing to the atom-by-atom resolution in this region with selected area diffraction, we can observe that, in the surface layer, implanted gold atoms form clusters with an ordered structure and an ordered region size of 2–3 nm. The interplanar distances (0.244 and 0.210 nm) determined from the selected area diffraction data correspond to slightly increased interplanar distances in the gold lattice for the (111) and (200) planes, respectively.

In the second zone with the layer thickness of approximately 60 nm, according to the results of the high-resolution transmission electron microscopy, there is an amorphous-like structural state (Fig. 4b), which is characteristic of oxides. The amorphization is also evidenced by the halo shape of the selected area diffraction pattern.

The third zone is characterized by a crystalline structure located at a depth of greater than 100 nm. It can be observed that, in this zone, there are phase inhomogeneities—at a depth of 130–100 nm, i.e., in crystalline layers closest to the surface, the composition of the crystallites is dominated by oxide phases, namely, TiO_2 and α-Al_2O_3, as well as by the AlN phase.

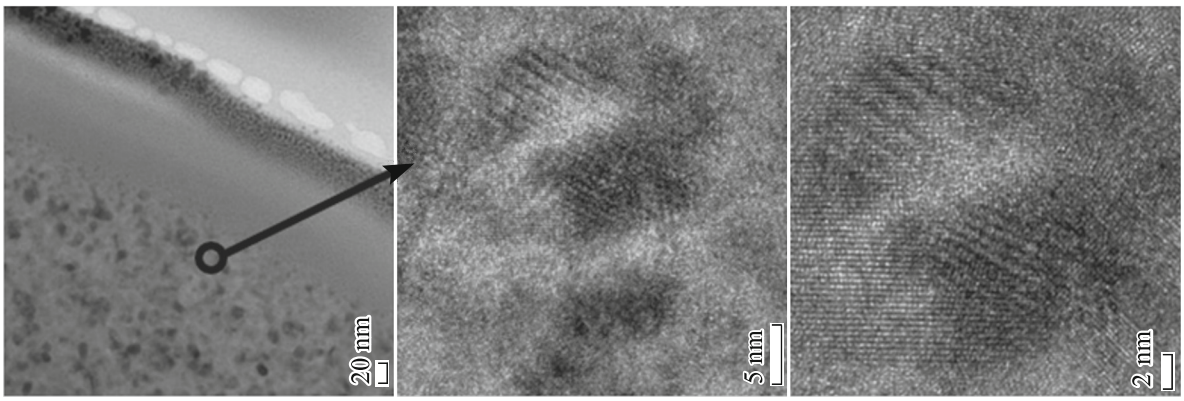

Fig. 5. High-resolution electron microscopy images with the selected area diffraction of the coating at a depth of 130 nm from the surface.

Deeper layers located at a depth of more than 130 nm (Fig. 5) retain the crystal structure after the high-temperature annealing (1300°C) of the sample.

4. CONCLUSIONS

Thus, the use of pulsed magnetron sputtering of a target with the complex composition $AlN–TiB_2–TiSi_2$ leads to the formation of a homogeneous amorphous-like coating with small droplet inclusions. This provides a high diffusion resistance to external influences due to the absence of easy diffusion paths.

The high-temperature annealing results in the formation of nanoscale phases Al_2O_3, AlB_2, AlN, and TiO_2. The implantation of Au^- ions with a dose of 10^{17} ions/cm^2 leads to the formation of an oxide (amorphous) sublayer with a thickness of 60 nm, as well as to the formation of Au^- nanoclusters of spherical shape in the near-surface layer.

ACKNOWLEDGMENTS

This study was performed within the framework of the Ukrainian complex state budget programs "Development of the Materials Science Basis for Structural Engineering of Vacuum Plasma Superhard Coatings with the Purpose of Achieving Desired Functional Properties" (project no. 0115U000682) and "Physical Principles of Plasma Technologies for Complex Processing of Multicomponent Materials and Coatings" (project no. 0113U000137c) and in collaboration with the National Institute for Materials Science (Tsukuba, Japan).

REFERENCES

1. D. P. Datta, Y. Takeda, H. Amekura, M. Sasase, and N. Kishimoto, Appl. Surf. Sci. **310**, 164 (2014).
2. A. D. Pogrebnjak and V. M. Beresnev, *Nanocoatings Nanosystems Nanotechnologies* (Bentham, Sharjah, United Arab Emirates, 2012).
3. A. D. Pogrebnyak, A. P. Shpak, N. A. Azarenkov, and V. M. Beresnev, Phys.—Usp. **52** (1), 29 (2009).
4. A. D. Pogrebnjak, G. Abadias, O. V. Bondar, O. V. Sobol, V. M. Beresnev, A. V. Pshyk, A. A. Demianenko, K. O. Belovol, D. A. Kolesnikov, and H. Komsta, Acta Phys. Pol., A **125** (6), 1284 (2014).
5. A. D. Pogrebnyak, A. A. Bagdasaryan, I. V. Yakushchenko, and V. M. Beresnev, Russ. Chem. Rev. **83** (11), 1027 (2014).
6. A. D. Pogrebnjak, D. Eyidi, G. Abadias, O. V. Bondar, V. M. Beresnev, and O. V. Sobol, Int. J. Refract. Met. Hard Mater. **48**, 222 (2015).
7. A. D. Pogrebnjak, I. V. Yakushchenko, A. A. Bagdasaryan, O. V. Bondar, R. Krause-Rehberg, G. Abadias, P. Chartier, K. Oyoshi, Y. Takeda, V. M. Beresnev, and O. V. Sobol, Mater. Chem. Phys. **147** (3), 1079 (2014).
8. A. D. Pogrebnyak, S. N. Bratushka, V. M. Beresnev, and N. Levintant-Zayonts, Russ. Chem. Rev. **82** (12), 1135 (2013).
9. V. Ivashchenko, S. Veprek, A. D. Pogrebnjak, and B. A. Postolnyi, Sci. Technol. Adv. Mater. **15**, 025007 (2014).

Translated by O. Borovik-Romanova